# Control Synthesis for a Class of Light and Agile Robotic Tensegrity Structures

J.B. Aldrich, R.E. Skelton
Dept. of Mechanical and Aerospace Engineering
University of California, La Jolla, CA 92093–0411

K. Kreutz-Delgado
Dept. of Electrical and Computer Engineering
University of California, La Jolla, CA 92093–0407

**Abstract**

For a new class of tendon-driven robotic systems that is generalized to include tensegrity structures, this paper focuses on a method to determine the tendon force inputs from a set of admissible, non-saturating inputs, that will move the rigid-body system from point A to point B along a prescribed path in minimum time. The approach utilizes the existence conditions and solution of a linear algebra problem that describes how the set of admissible tendon forces is mapped onto the set of path-dependent torques. Since this mapping is not one-to-one, free parameters in the control law always exist. An infinity-norm minimization with respect to these free parameters is responsible for saturation avoidance. Characterizing and optimizing these free parameters is the new contribution. Feedback is introduced to attenuate disturbances arising from the tensegrity paradigm. Examples illustrate methods and validate tensegrity's superior saturation avoidance capability.

## 1 Introduction

Robotic automation of repetitive assembly processes continues to gain more acceptance as an effective means to reduce labor costs and increase productivity in many manufacturing industries. This is especially true in pick-and-place applications where the objective is to move from one position to another quickly and accurately. As a result of driving the trajectories faster and faster, the inertial dynamics of typical robots become too large to be ignored, and therefore must be compensated by a feedback controller. Assuming that a sufficiently accurate plant model is available, the standard approach to this control problem is to implement a version of feedback linearization known as the computed-torque controller, [7–9,12]. *Theoretically*, this approach allows arbitrarily large configuration changes within the robot's workspace to occur quickly. As a practical matter, however, reconfiguration in near-zero time is not possible since the inertial forces to be carried by the actuators would have excessive magnitude causing actuator saturation. One way to circumvent this problem is to make the robot lose weight. For instance, a lighter design is possible by placing the heavy actuators at the base of the manipulator where a pulley-tendon system transmits torque remotely [8], Fig. (1a,b). Unfortunately, tendon compliance makes it difficult to transmit torque with sufficient bandwidth [5]. One approach that circumvents this problem is to design a mechanism that reduces tendon usage [13]. Alternatively, bandwidth can also be recovered by reducing system mass [4]. For instance, the tensegrity systems in Fig. (1c-h) can be designed with exceptionally low system mass and superior saturation avoidance capability since large bending moments normally present in the links get absorbed in the tendon network [10]. The work herein suggests that tensegrity concepts will revolutionize the manner in which tendon-driven systems are designed, controlled and utilized. We believe this will become especially true in environments where agile maneuvering and delicate object handling require a "soft" touch.

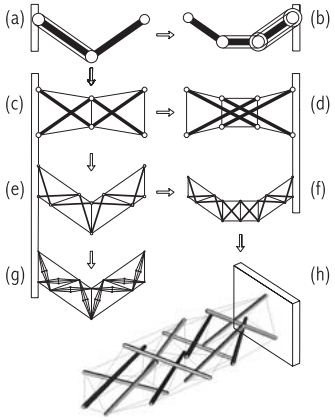


**Figure 1:** Proposed tensegrity robot evolution

In the sections that follow, we address the following questions: Given a set of admissible tendon forces, how should the control law be designed? For a given robot, which tendon network sustains more torque? What is its minimum-time trajectory along a prescribed path? How can feedback be used to keep it on track? Lastly, tensegrity model building methods and control simulations are illustrated by example.

## 2 Admissible tendon forces

A necessary condition for a tendon-driven robotic system is that all tendons be taut and unbroken. When this condition holds, we say that the tendon actuation system is in a state of unsaturation as follows.

**Definition 1** *An m-tendon actuation system is said to be* unsaturated *if* $t \in A$ *where*

$$A := \{t \in R^m : 0 < t_i < f_{yi},\}$$

*and* $t_i$ *is the tension in the* $i^{th}$ *tendon, and* $f_{yi}$ *is the yield force (max allowable tension) for the* $i^{th}$ *tendon. A system that is not* unsaturated, *is* saturated. *Set* $A$ *is the set of* admissible *tendon forces.*

## 3 Control problem statement

Given a desired reference trajectory, $q_d$, for a tendon-driven rigid-body system modelled as

$$M(q)\ddot{q} + V(q,\dot{q})\dot{q} + g(q) = G(q)t$$

($q \in R^n$, $t \in A \subset R^m$, $M$ is square), we seek to answer the question: Does there exist admissible tendon forces $t$ to yield the following closed loop system?

$$\ddot{z} + K_v\dot{z} + K_p z + K_i v = 0$$
$$z = q - q_d = \dot{v}$$

Yes, if and only if there exists $t \in A$ to solve

$$Gt = M(\ddot{q_d} - K_v\dot{z} - K_p z - K_i v) + V\dot{q} + g = \tau. \qquad (1)$$

There exists a $t \in R^m$ solving (1) iff $G_L\tau = 0$ where $G_L G = 0$ and $G_L G_L^T \succ 0$. If $t \in R^m$ exists to solve (1), then all solutions are given by

$$t = G^+\tau + G_R\eta \qquad (2)$$

where $GG_R = 0$ and $G_R^T G_R \succ 0$.

It is important to recognize two facts. First, the dimension of the nullspace of $G$ is $\rho(G) = m - \text{rank}(G)$. Hence, $\eta$ contains $\rho(G)$ free parameters that have neither been characterized nor optimized by the robotics community [1, 6, 8]. Second, even if a solution $t \in R^m$ exists there is no guarantee that there exists a choice for $\eta$ such that $t \in A$. An approach that resolves these facts is the main contribution of this paper.

## 4 How should free parameters be optimized?

In order to understand how to optimize the free parameters, $\eta$, a more suitable saturation definition is helpful. Toward this end, we introduce

$$D = \text{diag}\left[\, 2/f_{y1}\ 2/f_{y2}\ \cdots\ 2/f_{ym}\,\right]$$
$$e = \left[\, 1\ \cdots\ 1\,\right]^T, \quad t = \left[\, t_1\ \cdots\ t_m\,\right]^T$$

to establish a series of equivalent statements as follows.

**Theorem 1** *The following statements are equivalent:*

*(i) The m-tendon actuation system is* unsaturated.
*(ii) There exists a* $\delta < 1$ *such that* $\|Dt - e\|_\infty \le \delta$.
*(iii)* $t + d \in A$ *if* $\|d\|_\infty < (1-\delta)\min_i f_{yi}/2$.

**Corollary 1** *If the tendons are uniform, i.e.* $f_{yi} = f_y$ *for* $i = 1{:}m$, *then* $D^{-1}e = (f_y/2)e =: t_d$ *and the following statements are equivalent:*

*(i) The m-tendon actuation system is* unsaturated.
*(ii)* $\gamma := f_y/2 - \|t - t_d\|_\infty > 0$
*(iii)* $t + d \in A$ *if and only if* $\|d\|_\infty < \gamma$

**Proof:** *Thm.:* $t \in A$ holds iff $-(2/f_{yi})t_i + 1 < 1$ and $(2/f_{yi})t_i - 1 < 1$ for all $i = 1,\ldots,m$, which shows the *m*-tendon actuation system is *unsaturated* iff $\max\{|(2/f_{y1})t_1 - 1|, \ldots, |(2/f_{ym})t_m - 1|\} \le 1$. *Cor.:* $(ii) \Leftrightarrow \|t - t_d\|_\infty < f_y/2 \Leftrightarrow \|Dt - e\|_\infty < 1$ with $f_{yi} = f_y$ for $i = 1,\ldots,m$. If $(ii)$ holds, the perturbation force of least magnitude which causes either the onset of slackness or yield for the $i^{th}$ tendon has magnitude: $f_y/2 - |t_i - f_y/2|$. The saturating perturbation of least magnitude among all tendons has magnitude: $\min_i\{f_y/2 - |t_i - f_y/2|\} = f_y/2 - \max_i\{|t_i - f_y/2|\} = f_y/2 - \|t - (f_y/2)e\|_\infty = \gamma$. ■

In order to keep a tendon actuation system in a state of unsaturation that is robust to perturbations, $d$, we look to part (iii) of the corollary to motivate the following robust control objective.

**Robust control objective:** Maximize saturation margin, $\gamma$, w.r.t. free parameters in real-time.

An equivalent objective follows immediately from part $(ii)$ of the corollary: Minimize tendon force deviation from $t_d$ (50%-yield) w.r.t. free parameters in real-time,

$$\begin{aligned}\eta_\infty^* &:= \arg\min_{\eta} \|t(\eta) - t_d\|_\infty \\ &= \arg\min_{\theta,\eta}\ \theta \quad \text{s.t. } \theta \ge 0, \\ &\qquad -\theta e \le G^\perp\eta + G^+\tau - t_d \le \theta e\end{aligned}$$

where $t(\eta)$ is defined by (2) with the $G^\perp$ notation replacing $G_R$ hereafter. Alternatively, the free parameters can be computed as

$$\begin{aligned}\eta_2^* &:= \arg\min_{\eta} \|t(\eta) - t_d\|_2 \\ &= \arg\min_{\eta} \|G^\perp\eta + G^+\tau - t_d\|_2 = G^{\perp T} t_d\end{aligned}$$

where $G^\perp G^{\perp T} t_d$ is the orthonormal projection of $t_d$ into null($G$). The *least-squares minimizer*, $\eta_2^*$, can be expressed

analytically, and computed independent of the controller. In contrast, the *min-max minimizer*, $\eta^*_\infty$, requires a linear program, but is more effective for saturation avoidance.

**How effective is $\eta^*_\infty$ at saturation avoidance?** For a given torque loading, $\tau$, and robot geometry, $q$, the percent saturation, $S$, can be computed as a function of the free parameters, $\eta$, as

$$S(\eta) := (2/f_y)\|G^\perp(q)\eta + G^+(q)\tau - t_d\|_\infty \qquad (3)$$

In the example below, we illustrate how effective $\eta^*_\infty$ is at saturation avoidance in the presence of torque loading and a variable structure geometry.

**Example.** In Fig. (2) we are given two tendon actuation

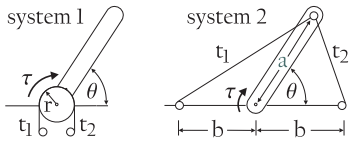


**Figure 2:** Benchmark comparison.

systems for a single link manipulator. The coupling matrices that map $t \in R^2$ into $\tau \in R^1$ for systems 1 and 2 are given respectively by

$$G_1 = r\begin{bmatrix} 1 & -1 \end{bmatrix}$$
$$G_2 = a\begin{bmatrix} -\frac{e\sin\theta}{\sqrt{c_1}} & \frac{e\sin\theta}{\sqrt{c_2}} \end{bmatrix}$$

where $c_1 = 1+e^2+2e\cos\theta$, $c_2 = c_1 - 4e\cos\theta$ and $e = b/a$. We let $a = \sqrt{3}/2$, $b = 1/2$, $r = 1/10$, and plot in Fig. (3) the level curves of percent saturation, $S(\eta^*_p)$, where $\eta^*_p$ is a function of $\tau$ and $\theta$. For instance,

$$\eta^*_\infty = \arg\min_\eta \left\| \begin{bmatrix} \sqrt{c_1} \\ \sqrt{c_2} \end{bmatrix} \eta + \begin{bmatrix} \frac{-0.5c_2\sqrt{c_1}}{(e+e^3)\sin\theta} \\ \frac{0.5c_1\sqrt{c_2}}{(e+e^3)\sin\theta} \end{bmatrix} \tau - \begin{bmatrix} \frac{f_y}{2} \\ \frac{f_y}{2} \end{bmatrix} \right\|_\infty$$

yields tendon forces $t = G_2^+\tau + G_2^\perp\eta^*_\infty$ for system 2. Figure (3b,c) shows the least-squares minimizer is slightly inferior to the minmax minimizer for saturation avoidance. Figure

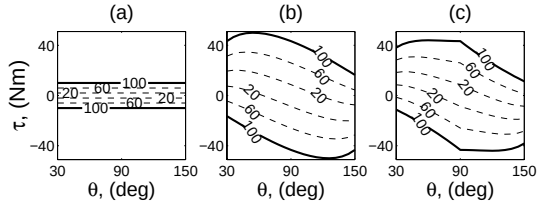


**Figure 3:** Level curves of percent saturation, $S(\eta^*_p)$, as a function of torque and geometry, $\tau$ and $\theta$. (a) system 1 with $p = \infty$, (b) system 2 with $p = \infty$, (c) system 2 with $p = 2$.

(3a,b) shows that system two is guaranteed to sustain greater torque than system one. ◇

The apparent *leverage advantage* of system two extends to most tensegrity systems as follows. Let $S_1$ denote $S(\eta^*_\infty)$ for pulley-based robots, Fig. (1a,b). Let $S_2$ denote $S(\eta^*_\infty)$ for tensegrity-based robots, Fig. (1c-h). The upper bounds on percent saturation,

$$\begin{aligned} S_1 &= (2/f_y)\|G^+\tau\|_\infty \\ &\le \left(\frac{\|\tau\|_\infty}{r}\right)\frac{2}{f_y} \\ S_2 &= (2/f_y)\|G^\perp\eta^*_\infty - t_d + G^+\tau\|_\infty \\ &\le \left(k_1(q) + k_2(q)\frac{\|\tau\|_\infty}{a}\right)\frac{2}{f_y} \end{aligned}$$

validate tensegrity's *leverage advantage* for most configurations where $k_1 \approx 0$, $k_2 \approx 1$ and the link lengths are sufficiently greater than the pulley radii, i.e. $a \gg r$. Increasing the sustainable torque means point-to-point maneuvering can occur in less time.

## 5 Minimum-time control along a path

Given a rigid-body system, a tendon network and a path, we pose the following problem statement:

*What admissible tendon force inputs will move plant from point A to point B along a prescribed path in minimum time?*

The solution is broken down into three tasks: First, convert the free dynamics to the *path-following dynamics*. Second, substitute the path-following dynamics into the tendon saturation constraint to get a *path-acceleration constraint*. Third, construct the *minimum-time solution* by maximizing the path velocity at each point on path [2].

**Path-following dynamics.** The rigid-body free dynamics are expressed as, $M(q)\ddot{q} + h(q,\dot{q}) = \tau$. For *kinematically-invertible* robots/tensegrities, the tip of the manipulator can be written as an explicit function of the joint angles or the distance along the path:

$$r(q) = \tilde{r}(s)$$

Differentiating w.r.t. time yields

$$r_q\dot{q} = \tilde{r}_s\dot{s}$$
$$r_q\ddot{q} + \dot{r}_q\dot{q} = \tilde{r}_s\ddot{s} + \tilde{r}_{ss}\dot{s}^2$$

where $r_q = \partial r/\partial q$ is the Jacobian. We now can compute $q = q(s)$, $\dot{q} = \dot{q}(s,\dot{s})$, $\ddot{q} = \ddot{q}(s,\dot{s},\ddot{s})$ and the *path-following dynamics* as

$$\begin{aligned} \tau(s,\dot{s},\ddot{s}) &= u(s)\ddot{s} + v(s,\dot{s}) \qquad (4) \\ u(s) &= M(q)r_q^{-1}\tilde{r}_s \\ v(s,\dot{s}) &= M(q)r_q^{-1}(\tilde{r}_{ss}\dot{s}^2 - \dot{r}_q\dot{q}) + h(q,\dot{q}) \end{aligned}$$

**Path-acceleration constraint.** Recall the linear algebra problem: $\tau(s,\dot{s},\ddot{s}) = G(s)t$ whose solution $t = G^{+}\tau + G^{\perp}\eta$ exists iff $[I - GG^{+}]\tau = 0$. Assuming solution exists (which is true automatically when $G$ is full row rank), substitute it into the tendon saturation constraint of theorem 1, $\|Dt - e\|_{\infty} \leq \delta$, to get

$$\|a(s,\dot{s},\eta) + \ddot{s}c(s)\|_{\infty} \leq \delta$$

where $a = DG^{\perp}\eta + DG^{+}v - e$ and $c = DG^{+}u$. Equivalently, we get $-\delta \leq a_i(s,\dot{s},\eta) + \ddot{s}c_i(s) \leq \delta$ for $i = 1$ to $m$. Rearrangement yields *path-acceleration constraint*,

$$\begin{aligned} f(s,\dot{s},\eta) \leq \ddot{s} \leq g(s,\dot{s},\eta) \\ f = \max_i ((-\text{sign}(c_i)\delta - a_i)/c_i) \\ g = \min_i ((\text{sign}(c_i)\delta - a_i)/c_i) \end{aligned}$$

**Minimum-time solution.** The minimum-time solution is obtained by choosing the acceleration $\ddot{s}$ to make the velocity $\dot{s}$ as large as possible at every point $s$ without violating $f(s,\dot{s},\eta) \leq g(s,\dot{s},\eta)$. This follows by minimizing the cost,

$$J = \int_0^T dt = \int_A^B \frac{1}{\dot{s}(s)} ds$$

In [2], it was shown that $J$ is minimized if and only if $\ddot{s}$ always takes either its largest or its smallest admissible value. In summary, it is easy to show the following.

**Theorem 2** *The path-following minimum time solution subject to $t \in A$ is obtained by switching between maximum acceleration, $\ddot{s} = g(s,\dot{s},\eta^{*}_{\infty})$, and maximum deceleration $\ddot{s} = f(s,\dot{s},\eta^{*}_{\infty})$ where $\eta^{*}_{\infty} = \arg\min_{\eta} \|A(s)\eta + b(s,\dot{s}) + \ddot{s}c(s)\|_{\infty}$ and $A = DG^{\perp}$, $b = DG^{+}v - e$, $c = DG^{+}u$.*

**Corollary 2** *The path-following minimum time solution subject to $t \in A$ and $\min_{\eta} \|Dt(\eta) - e\|_2$ is obtained by switching between $\ddot{s} = g(s,\dot{s},\eta^{*}_{2})$ and $\ddot{s} = f(s,\dot{s},\eta^{*}_{2})$ where $\eta^{*}_{2} = G^{\perp T}(s)D^{-1}e$.*

The remaining task is to determine when to switch between $f$ and $g$. Techniques for locating switching points are described in [2, 11] and applied to an example at the end of the paper. The minimum time solution yields the desired open-loop trajectory, $q_d$. Feedback can be used to reduce the tracking error, $z = q - q_d$, as discussed next.

## 6 Model uncertainty and feedback control

For the uncertain plant, $M(q)\ddot{q} + V(q,\dot{q})\dot{q} + g(q) + d_w = G\hat{t}$, we compute $\hat{t} = \hat{G}^{\perp}\eta + \hat{G}^{+}\hat{\tau} + u_r$ as the feedback law where $u_r$ is a robust control input, $d_w$ is an external disturbance and $G = G(q)$ is assumed. Three sources of parametric uncertainty are considered here, namely, the *standard error*, $\tilde{\tau} = \tau - \hat{\tau}$, that occurs in all robotic systems, and two tensegrity-based errors,

$$\begin{aligned} \tilde{G}^{+} &= G^{+} - \hat{G}^{+} \quad \textit{psuedoinverse error} \\ \tilde{G}^{\perp} &= G^{\perp} - \hat{G}^{\perp} \quad \textit{nullspace error} \end{aligned}$$

Assuming $q$ is measured exactly and $G$ is full row rank, the closed loop system becomes $M(q)\ddot{q} + V(q,\dot{q})\dot{q} + g(q) + d_t = \tau + Gu_r$, where the total disturbance is $d_t = d_w + G\tilde{G}^{+}\tau + G\tilde{G}^{\perp}\eta + G\hat{G}^{+}\tilde{\tau}$.

**Lyapunov design.** Given time-optimal reference trajectories how do we stay on path using feedback? This can be solved by using a Lyapunov function: $V_1 = \frac{1}{2}r^T M(q)r$ where $r = \Lambda z + \dot{z}$. First, we can rewrite dynamics in terms of filtered tracking error $r$ as, $M(q)\dot{r} = Y(\cdot)\phi - V(q,\dot{q})r - d_t + \tau + Gu_r$, where $Y(\cdot)\phi = M(q)(\Lambda\dot{z} - \ddot{q}_d) + V(q,\dot{q})(\Lambda z - \dot{q}_d) - g(q)$. Then we choose nominal input as $\tau = -Y(\cdot)\phi - K_r r$ with error $\tilde{\tau} = -Y(\cdot)\tilde{\phi}$. The robust input, $u_r = k_d\hat{G}^{+}\text{sgn}(r)$ can be implemented without error since we assume the state is known exactly. The psuedoinverse error is bounded as $-\bar{g}I \leq G\tilde{G}^{+} \leq \bar{g}I$, where $0 \leq \bar{g} \leq 1$. The time-derivative of the Lyapunov function becomes,

$$\begin{aligned} \dot{V}_1 &= r^T M(q)\dot{r} + r^T \dot{M}(q)r/2 \\ &= r^T(Y(\cdot)\phi - d_t + \tau + Gu_r) \\ &\quad + r^T(\dot{M}(q)/2 - V(q,\dot{q}))r \\ &= r^T(Y(\cdot)\phi - d_t + \tau + Gu_r) \\ &= -r^T K_r r - r^T d_t + r^T G u_r \\ &= -r^T K_r r - r^T d_t + (k_d + \bar{g}|k_d|)\sum_{i=1}^{n} |r_i| \\ &\leq -r^T K_r r + \sum_{i=1}^{n} |r_i||d_{ti}| + (k_d + \bar{g}|k_d|)\sum_{i=1}^{n} |r_i| \\ &\leq -r^T K_r r + \sum_{i=1}^{n} |r_i| \left( \max_i |d_{ti}| + k_d + \bar{g}|k_d| \right) \\ &\leq -r^T K_r r \quad \text{if } k_d = -|k_d|, \quad |k_d| \geq \frac{||d_t||_{\infty}}{(1-\bar{g})} \end{aligned} \tag{5}$$

If the robust control gain requirement in (5) holds, then $\dot{V}_1 \leq 0$ and a La Salle's argument given in [7] can be used to show that the tracking errors are asymptotically stable. (The skew-symmetric property is used to simplify equality 2 above. For equality 4, use $r^T G u_r = k_d r^T G\hat{G}^{+}\text{sgn}(r) = k_d r^T \text{sgn}(r) - k_d r^T G\tilde{G}^{+}\text{sgn}(r) \leq (k_d + \bar{g}|k_d|)\sum_{i=1}^{n} |r_i|$ to simplify.)

The gain requirement on $|k_d|$ can be reduced with the adaptive inertial-related control [7]. Finite-bandwidth robust control is possible by replacing the sign function with a saturation function in $u_r$ [9]. For standard non-tensegrity robots, (5) reduces to $|k_d| \geq ||d_w + \tilde{\tau}||_{\infty}$.

## 7 Tensegrity Model

In this section, a family of dynamical system models is generated for a generalized class of tendon-driven robots that includes tensegrity structures. First, the rigid body dynamic models for serial-link and free-link systems are developed. Second, tendon actuation model building is conveyed by an illustrative example.

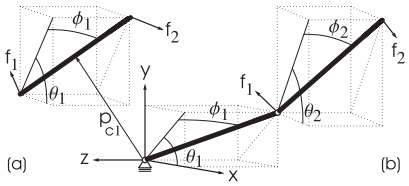


**Figure 4:** (a) Free-link. (b) Serial-link.

**Serial-link model.** The geometry of a serial-link rigid-body system with $b$ bars (links) is shown in Fig. (4b) for the two-bar case. For convenience, its $n$ degrees of freedom are organized as

$$q = \begin{bmatrix} q_1^T & q_2^T & \cdots & q_b^T \end{bmatrix}^T \in R^n, \quad q_i = \begin{bmatrix} \theta_i & \phi_i \end{bmatrix}^T$$

The position of the $i^{th}$ bar's tip, $p_i$, and center of mass, $p_{ci}$, are expressed in terms of $q$ as follows

$$p_i = p_o + \sum_{k=1}^{i} a_k \beta_k$$
$$p_{ci} = p_o + \sum_{k=1}^{i-1} a_k \beta_k + a_{ci} \beta_i \qquad \beta_i = \begin{bmatrix} c\theta_i c\phi_i \\ s\theta_i c\phi_i \\ -s\phi_i \end{bmatrix}$$

where $c(\cdot) = \cos(\cdot)$, $s(\cdot) = \sin(\cdot)$, $a_i$ is the length of the $i^{th}$ bar, and $a_{ci}$ is the distance from node to center of mass. Time-derivative of position yields velocities,

$$\dot{p}_i = \sum_{k=1}^{i} a_k \frac{\partial \beta_k}{\partial q_k} \dot{q}_k =: \Psi_i(q)\dot{q}$$
$$\dot{p}_{ci} = \sum_{k=1}^{i-1} a_k \frac{\partial \beta_k}{\partial q_k} \dot{q}_k + a_{ci} \frac{\partial \beta_i}{\partial q_i} \dot{q}_i =: \Psi_{ci}(q)\dot{q}$$

where $(3 \times n)$ matrices, $\Psi_i(q) = \begin{bmatrix} J_1 & J_2 & \cdots & J_i & O_{ni} \end{bmatrix}$ and $\Psi_{ci}(q) = \begin{bmatrix} J_1 & J_2 & \cdots & J_{i-1} & J_{ci} & O_{ni} \end{bmatrix}$, consist of Jacobians, $J_i = a_i \partial \beta_i / \partial q_i$ and $J_{ci} = a_{ci} \partial \beta_i / \partial q_i$, and a matrix of zeros with $n - 2i$ columns, $O_{ni}$. The kinetic energy for the rigid body system becomes

$$K = \frac{1}{2} \sum_{i=1}^{b} (m_i \dot{p}_{ci}^T \dot{p}_{ci} + \dot{q}_i^T I_i(q_i) \dot{q}_i) \tag{6}$$
$$= \frac{1}{2} \dot{q}^T \left[ \sum_{i=1}^{b} m_i \Psi_{ci}^T(q) \Psi_{ci}(q) + I(q) \right] \dot{q} =: \frac{1}{2} \dot{q}^T M(q) \dot{q}$$

where $I = \text{diag}\begin{bmatrix} I_1 & I_2 & \cdots & I_b \end{bmatrix} \in R^{n \times n}$, consists of inertial blocks, $I_i = \text{diag}\begin{bmatrix} \frac{m_i}{12}(a_i c\phi_i)^2 & \frac{m_i}{12} a_i^2 \end{bmatrix}$. Notice how the kinetic energy derivation yields the mass matrix as a freebee! The potential energy for the rigid body system is

$$V = \sum_{i=1}^{b} p_{ci}^T f_{gi}, \quad f_{gi} = \begin{bmatrix} 0 & m_i g & 0 \end{bmatrix}^T$$

The kinetic and potential energies are differentiated in Lagrange's equations of motion,

$$\frac{d}{dt} \frac{\partial K}{\partial \dot{q}} - \frac{\partial K}{\partial q} + \frac{\partial V}{\partial q} = \tau$$

and rearranged into the following matrix form [12],

$$M(q)\ddot{q} + V(q,\dot{q})\dot{q} + g(q) = \tau$$

Specifically, if we denote the mass and coriolis/centripetal matrices elementwise as $M = [\mu_{kj}]$ and $V = [\zeta_{kj}]$, then $V$ can be completely determined from $M$ using the following Christoffel parameters [12],

$$\zeta_{kj} = \frac{1}{2} \sum_{i=1}^{n} \left( \frac{\partial \mu_{kj}}{\partial q_i} + \frac{\partial \mu_{ki}}{\partial q_j} - \frac{\partial \mu_{ij}}{\partial q_k} \right) \dot{q}_i \tag{7}$$

The gravity-induced torque vector becomes

$$g(q) := \frac{\partial V}{\partial q} = \sum_{i=1}^{b} \left( \frac{\partial p_{ci}}{\partial q} \right)^T f_{gi} = \sum_{i=1}^{b} \Psi_{ci}^T f_{gi}$$

Nodal forces, $f = \begin{bmatrix} f_1^T & f_2^T & \cdots & f_b^T \end{bmatrix}^T$, in cartesian space, $f_i \in R^3$, are induced by the tendon actuation system. Using the principle of virtual work [12], the mapping from nodal forces, $f \in R^{3b}$, to torques, $\tau \in R^n$, is

$$\tau = \sum_{i=1}^{b} \Psi_i^T f_i = \begin{bmatrix} \Psi_1^T & \Psi_2^T & \cdots & \Psi_b^T \end{bmatrix} f =: H(q) f$$

**Free-link model.** For tensegrity structures designed with inertially-isolated rigid bars as depicted in Fig. (4a), a single bar has five degrees of freedom–three translations of its mass center, $p_{c1} \in R^3$, and two Euler angles, $q_1 \in R^2$. Using (6) with $b = 1$, the kinetic energy of a single free link is

$$K = \frac{1}{2}(m_1 \dot{p}_{c1}^T \dot{p}_{c1} + \dot{q}_1^T I_1(q_1) \dot{q}_1)$$
$$= \frac{1}{2} \begin{bmatrix} \dot{p}_{c1}^T & \dot{q}_1^T \end{bmatrix} \begin{bmatrix} m_1 I & 0 \\ 0 & I_1(q_1) \end{bmatrix} \begin{bmatrix} \dot{p}_{c1} \\ \dot{q}_1 \end{bmatrix} =: \frac{1}{2} \dot{q}^T M(q) \dot{q}$$

Notice that $q$ is now a 5-vector, not a 2-vector as before. Use (7) again to get $V(q,\dot{q})$ from $M(q)$. The gravity vector, $g(q) = \begin{bmatrix} I & 0 \end{bmatrix}^T f_{g1}$ is trivial. Using the principle of virtual work, this nodal force to torque mapping becomes

$$\tau = \begin{bmatrix} I & I \\ -J_{c1}^T & J_{c1}^T \end{bmatrix} \begin{bmatrix} f_1 \\ f_2 \end{bmatrix} =: H(q) f$$



Proceedings of the American Control Conference
Denver, Colorado June 4-6, 2003

## 8 Illustrative Examples

In this section, models for two different plants are generated and a minimum-time control simulation is given to illustrate the simplicity, scope, and potential of light and agile robotic tensegrity structures.

**Plant 1.** Two inertially-isolated double-link manipulators interconnected with flexible tendons are shown in figure (5). This system can be described by two copies of the serial-link

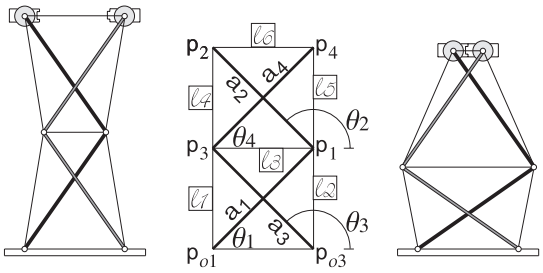


**Figure 5:** Tensegrity robot joining two workpieces.

model where $b=2$, $n=2$ and $\phi_i=0$ for each copy. Combining the copies yields

$$M(q)\ddot{q}+V(q,\dot{q})\dot{q}+g(q)=H(q)f \tag{8}$$

as the global model where

$$M=\mathrm{diag}\left[M_{12}\ M_{34}\right],\quad V=\mathrm{diag}\left[V_{12}\ V_{34}\right]$$
$$H=\begin{bmatrix}H_{12}&\\&H_{34}\end{bmatrix},\quad q=\begin{bmatrix}q_{12}\\q_{34}\end{bmatrix},\quad f=\begin{bmatrix}f_{12}\\f_{34}\end{bmatrix}$$
$$M_{ij}=\begin{bmatrix}m_ia_{ci}^2+m_ja_{cj}^2+I_{\theta i} & m_ja_{cj}a_i(\mathrm{c}\theta_{ij})\\ m_ja_{cj}a_i(\mathrm{c}\theta_{ij}) & m_ja_{cj}^2+I_{\theta j}\end{bmatrix}$$
$$V_{ij}=\begin{bmatrix}0 & -m_ja_{cj}a_i(\mathrm{s}\theta_{ij})\dot{\theta}_j\\ m_ja_{cj}a_i(\mathrm{s}\theta_{ij})\dot{\theta}_i & 0\end{bmatrix}$$
$$H_{ij}=\begin{bmatrix}J_i^T & J_i^T\\ 0 & J_j^T\end{bmatrix},\quad J_i^T=a_i\left[-\mathrm{s}\theta_i\ \mathrm{c}\theta_i\right]$$

and $\theta_{ij}=\theta_j-\theta_i$, $q_{ij}=\left[\theta_i\ \theta_j\right]^T$, $f_{ij}=\left[f_i^T\ f_j^T\right]^T$, $\mathrm{s}\theta_i=\sin\theta_i$, $\mathrm{c}\theta_i=\cos\theta_i$. Gravity acts orthogonal to the plane of motion, and therefore $g=0$. The nodal points, $p_i$, are computed using forward kinematics,

$$p_i=p_{oi}+a_i\begin{bmatrix}\mathrm{c}\theta_i\\ \mathrm{s}\theta_i\end{bmatrix},\quad p_{i+1}=p_i+a_{i+1}\begin{bmatrix}\mathrm{c}\theta_{i+1}\\ \mathrm{s}\theta_{i+1}\end{bmatrix}$$

where $i=1$ for the first 2-link arm and $i=3$ for the second 2-link arm. The tendon orientation vectors, $\ell_i$, are defined in terms of the nodal points as

$$\begin{bmatrix}\ell_1\\ \ell_2\\ \ell_3\\ \ell_4\\ \ell_5\\ \ell_6\end{bmatrix}=\left[\begin{array}{cc|cccc}-I & & & & I & \\ & I & & & & \\ \hline -I & & & & I & \\ & & -I & I & & \\ -I & & & & & I\\ & & & -I & I & \end{array}\right]\begin{bmatrix}p_{o1}\\ p_{o3}\\ \hline p_1\\ p_2\\ p_3\\ p_4\end{bmatrix}=C_op_o+Cp$$

which is used to compute the direction cosine matrix, $D=\mathrm{diag}(\left[d_1\ d_2\ d_3\ d_4\ d_5\ d_6\right])$ where $d_i=\ell_i(\ell_i^T\ell_i)^{-1/2}$. The principle of virtual work yields $f=C^TD(q)t$. The rigid-body and tendon-actuation systems are joined as

$$M(q)\ddot{q}+V(q,\dot{q})\dot{q}+g(q)=G(q)t,\qquad G:=HC^TD$$
$$G=\begin{bmatrix}0 & -J_1^Td_2 & -J_1^Td_3 & -J_1^Td_4 & -J_1^Td_5 & -J_1^Td_6\\ 0 & 0 & 0 & -J_2^Td_4 & 0 & -J_2^Td_6\\ J_3^Td_1 & 0 & J_3^Td_3 & J_3^Td_4 & J_3^Td_5 & J_3^Td_6\\ 0 & 0 & 0 & 0 & J_4^Td_5 & J_4^Td_6\end{bmatrix}$$

It is easy to see when $G\in R^{4\times6}$ drops rank, since $J_i^Td_j=0$ if and only if tendon $j$ is unattached or colinear to bar $i$.

**Plant 2.** A two-stage tensegrity-based manipulator shown in figure (6). This system can be described by three copies of

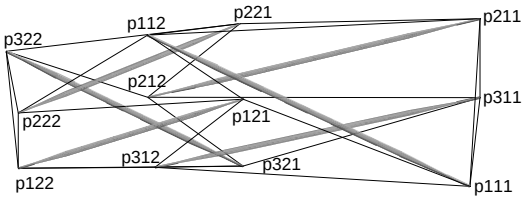


**Figure 6:** 3D tensegrity robot fixed at $p_{111}$, $p_{211}$ and $p_{311}$.

the serial-link model with $b=1$ and $n=2$, and three copies of the free-link model. Assuming zero-gravity yields $g=0$ and the global model (8) as

$$M=\mathrm{diag}\left[M_{11}\ M_{21}\ M_{31}\ M_{12}\ M_{22}\ M_{32}\right]$$
$$V=\mathrm{diag}\left[V_{11}\ V_{21}\ V_{31}\ V_{12}\ V_{22}\ V_{32}\right]$$
$$H=\mathrm{diag}\left[H_{11}\ H_{21}\ H_{31}\ H_{12}\ H_{22}\ H_{32}\right]$$
$$q=\left[q_{11}^T\ q_{21}^T\ q_{31}^T\ q_{12}^T\ q_{22}^T\ q_{32}^T\right]^T,\quad q_{i1}=\sigma_{i1}$$
$$f=\left[f_{11}^T\ f_{21}^T\ f_{31}^T\ f_{12}^T\ f_{22}^T\ f_{32}^T\right]^T,\quad f_{i1}=f_{i12}$$
$$q_{i2}=\left[p_{ci}^T\ \sigma_{i2}^T\right]^T,\quad f_{i2}=\left[f_{i21}^T\ f_{i22}^T\right]^T$$
$$M_{i1}=4I_{i1},\quad V_{i1}=4C_{i1},\quad H_{i1}=2J_{i1}$$
$$M_{i2}=\mathrm{diag}\left[m_{ij}I\ I_{i2}\right],\quad V_{i2}=\mathrm{diag}\left[0\ C_{i2}\right]$$
$$H_{i2}=\begin{bmatrix}I & I\\ -J_{i2} & J_{i2}\end{bmatrix},\quad I_{ij}=\frac{m_{ij}a_{ij}^2}{12}\begin{bmatrix}(\mathrm{c}\phi_{ij})^2 & 0\\ 0 & 1\end{bmatrix}$$
$$C_{ij}=\frac{m_{ij}a_{ij}^2\mathrm{s}\phi_{ij}\mathrm{c}\phi_{ij}}{12}\begin{bmatrix}-\dot{\phi}_{ij} & -\dot{\theta}_{ij}\\ \dot{\theta}_{ij} & 0\end{bmatrix}$$
$$J_{ij}=\frac{a_{ij}}{2}\begin{bmatrix}-\mathrm{s}\theta_{ij}\mathrm{c}\phi_{ij} & \mathrm{c}\theta_{ij}\mathrm{c}\phi_{ij} & 0\\ -\mathrm{c}\theta_{ij}\mathrm{c}\phi_{ij} & \mathrm{s}\theta_{ij}\mathrm{s}\phi_{ij} & -\mathrm{c}\phi_{ij}\end{bmatrix}$$

Euler-angles are denoted by $\sigma_{ij}=\left[\theta_{ij}\ \phi_{ij}\right]^T$. Nodal force $f_{ijk}\in R^3$ is applied to node $p_{ijk}\in R^3$ where

$$p_{i12}=p_{i11}+a_{i1}\beta_{i1}$$
$$p_{i21}=p_{ci}-(a_{i2}/2)\beta_{i2}$$
$$p_{i22}=p_{ci}+(a_{i2}/2)\beta_{i2}$$
$$\beta_{ij}=\begin{bmatrix}\mathrm{c}\theta_{ij}\mathrm{c}\phi_{ij}\\ \mathrm{s}\theta_{ij}\mathrm{c}\phi_{ij}\\ -\mathrm{s}\phi_{ij}\end{bmatrix}$$

for $i = 1,2$ and 3. The nodal points, tendon orientation vectors, direction cosines and $G$ are computed in the same manner as in the previous example.

**Simulation.** The minimum-time tendon forces are designed for the two-link serial manipulator pictured in (1a). The tendon forces illustrated in figure (7a) are designed to move the manipulator tip along a specific path, i.e. $x = 4(s-0.5)^3$ and $y = s+5$, in minimal time according to corollary 2. Four tendons are used, but only two of them are illustrated in the figure, since $t_2 = f_y - t_1$ and $t_4 = f_y - t_3$ due to symmetry in the tendon network. The phase plane trajectory, i.e. $\ddot{s}$ versus

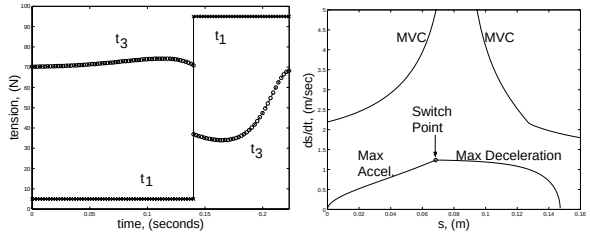


**Figure 7:** (a) Time-optimal tendon force trajectories for $5 \leq t \leq 95$N with switching point at 0.14 sec. (b) Maximum Velocity Curve (MVC) and optimal path trajectory.

$s$, for this design is illustrated in figure (7b). Clearly, the control input is feasible since it is bounded above by the maximum velocity curve. The switching point indicates where on the path the maximum path-acceleration, g, is switched to the maximum path-deceleration, f. See [2, 11] for algorithm details. This procedure can be repeated for plants 1 and 2 by prescribing a feasible path for all degrees of freedom.

**Tension rate constraint.** Notice in figure (7a) the tendon forces are discontinuous at the switching point. Since tendons have finite bandwidth, the control law must be smoothened for implementation. Smooth minimum-time trajectories are computed by using the algorithm given in [3] to ensure tension rates, $\dot{t}$, instead of torque rates, $\dot{\tau}$, are bounded. This substitution is straightforward once we express $\dot{t}$ in *exactly* the same form as $\dot{\tau}$ as follows

$$\begin{aligned} \dot{t} &= \vartheta(s)\dddot{s} + \lambda(s,\dot{s},\ddot{s}), \qquad \dot{t} \in R^m \\ \dot{\tau} &= \upsilon(s)\dddot{s} + \nu(s,\dot{s},\ddot{s}), \qquad \dot{\tau} \in R^n. \end{aligned} \tag{9}$$

To derive $\vartheta$, $\lambda$, $\upsilon$ and $\nu$, we first define $\kappa_i$ as the $i^{th}$ column of $G^+ \in R^{m\times n}$, $\gamma_i$ as the $i^{th}$ column of $G^\perp \in R^{m\times\rho}$, and note that [3] shows how $\tau$ in (4) can be differentiated to get $\upsilon$ and $\nu$ in (9). Then, $\lambda = \sum_{i=1}^{n}(\tau_i \frac{\partial \kappa_i}{\partial q}\dot{q} + \nu_i\kappa_i) + \sum_{i=1}^{\rho}(\eta_i \frac{\partial \gamma_i}{\partial q}\dot{q} + \dot{\eta}_i\gamma_i)$ and $\vartheta = \sum_{i=1}^{n}\upsilon_i\kappa_i$, where the elements of $\tau$, $\nu$, $\eta$, $\dot{\eta}$ and $\upsilon$ are denoted by subscript $i$. To keep $\lambda$ independent of $\dddot{s}$, we use the *least-squares minimizer*, $\eta = (f_y/2)G^{\perp T}e \in R^\rho$, which yields $\eta_i = (f_y/2)\sum_{j=1}^{m}\gamma_{ij}$ and $\dot{\eta}_i = (f_y/2)\sum_{j=1}^{m}\frac{\partial \gamma_{ij}}{\partial q}\dot{q}$. All trajectories are smooth because [3] uses cubic splines to parameterize $\dot{s}(s)$.

## 9 Conclusion

This paper describes a feedback linearization control law that uses the parameters in the nullspace of the control distribution matrix, $G$, to minimize the norm of the tendon force tracking error, $\|t - t_d\|$, while avoiding saturation of the control signals. This paper has also shown that when the free parameters in the tendon control law are optimized in real-time, control synthesis for a generalized class of light and agile robotic tensegrity structures is possible. Future work will focus on integrating structure and control design so that optimal candidates within this new robotics paradigm can be identified on a task-by-task basis.

## References


[1] A. Bicchi and D. Prattichizzo. "Analysis and optimization of tendinous actuation for biomorphically designed robotic systems". *Robotic systems*, 2000-1.

[2] J.E. Bobrow, S. Dubowsky, and J.S. Gibson. "Time-Optimal Control of Robotic Manipulators Along Specified Paths". *Int J of Robot Res*, 4(3), 1985.

[3] D. Constantinescu and E.A. Croft. "Smooth and Time-Optimal Trajectory Planning for Industrial Manipulators along Specified Paths". *J Robot Sys*, 2000.

[4] V. Hayward and J. Cruz-Hernandez. "Parameter sensitivity analysis for design and control of tendon transmission". *Experimental Robotics*, 1995.

[5] C. Johnstun and C. Smith. "Modelling and design of a mechanical tendon actuation system". *ASME Trans J Dyn Sys Meas Control*, 1992.

[6] H. Kobayashi, K. Hyodo, and D. Ogane. "On intellegent control of tendon-driven robotic mechanisms with redundant tendons". *Int J Robot Res*, 17(5):561–571, 1998.

[7] F.L. Lewis, C.T. Abdallah, and D.M. Dawson. *Control of Robotic Manipulators*. Macmillian, 1993.

[8] R. Murray, Z. Li, and S. Sastry. *A Mathematical Introduction to Robotic Manipulation*. CRC Press, 1994.

[9] Z. Qu and D.M. Dawson. *Robust Tracking Control of Robot Manipulators*. IEEE Press, 1996.

[10] R.E. Skelton, J.W. Helton, R. Adhikari, J. Pinaud, and W. Chan. "An introduction to the mechanics of tensegrity structures". In *Conference on Decision and Control*, volume 5, pages 4254–9, 2001.

[11] J.-J. E. Slotine and H. Yang. "Improving the Efficiency of Time-Optimal Path-Following Algorithms". *IEEE Trans Robot Automat*, 5(1):118–124, 1989.

[12] M. Spong and M. Vidyasagar. *Robot Dynamics and Control*. Wiley, 1989.

[13] W.T. Townsend and J.A. Guertin. "Teleoperator slave - W.A.M. design methodology". *Industrial Robot*, 26(3):167–177, 1999.